Journal of Manufacturing Processes 98 (2023) 216–222

Contents lists available at ScienceDirect

Journal of Manufacturing Processes

journal homepage: www.elsevier.com/locate/manpro

Bi-metal structures fabricated by extrusion-based sintering-assisted additive manufacturing

Dayue Jiang, Fuda Ning *

Department of Systems Science and Industrial Engineering, State University of New York at Binghamton, Binghamton, New York 13902, USA

ARTICLE INFO

Keywords:
Bi-metal structures
Material extrusion
Sintering
Inconel 625
17–4 PH stainless steel

ABSTRACT

The manufacturing of bi-metal structure has received much interest because it provides compensated properties for a single metal alloy, meeting the harsh requirements for components used in key industries like aerospace, defense, energy, etc. Additive manufacturing (AM) has been extensively applied in building multi-material structures because of its ability to vary material type and composition in a layer-by-layer mode. However, fusion-based AM technologies usually induce interfacial cracks and delamination resulted from the large mismatch of coefficient of thermal expansion (CTE) between dissimilar materials, while the solid-state AM methods generate a large number of pores at the interface, requiring post-fabrication heat treatment. In this study, we aim to build high-quality 17–4 PH stainless steel and nickel alloy bi-metal structure with material extrusion AM method, followed by debinding and sintering processes. The microstructure and mechanical properties of the bi-metal structure were thoroughly investigated. It was revealed that small pores were distributed in the whole part, and no brittle intermetallic phase but slightly larger pores were formed at the interface. The material transition zone was relatively small in thickness, exhibiting low bonding strength and low hardness but a ductile deformation behavior. The completion of this study provides a pioneering analysis of bi-metal structures built by extrusion-based sintering-assisted AM, and shows a great promise for further adoption of this technology in a variety of industrial applications.

1. Introduction

Combining dissimilar metal materials for hybrid structure has gained increasing interest to fill the demand for a variety of industrial applications. The advantages of bi-metal structure include better structural performance, higher mechanical strength, and higher economic efficiency compared with single metal alloy parts [1]. For example, stainless steel (SS) and nickel-based super alloys have been joined for the fabrication of high-temperature components for gas turbine engines, nuclear plants, and water reactors [2]. Such a combination takes advantage of the high mechanical strength and corrosion resistance from stainless steel while integrates the great high-temperature performance of the nickel-based superalloys [3]. Bi-metal components can also incorporate other material properties such as electronic conductivity, thermal conductivity, wear resistance, and magnetism [4,5]. The successful fabrication of such bi-metal structures significantly expands the material selection for specific industrial applications.

Additive manufacturing (AM) has become a widespread technology to build metallic components due to its freeform design and rapid prototyping capability. It is also suitable for multi-material fabrication by layering one type of material over another. For joining dissimilar metal material using AM, two different approaches are usually utilized, including fusion-based AM and solid-state AM processes. During fusion-based AM processes, a high-energy power source, e.g., laser, wire arc, or electron beam, is applied to melt the feedstock material, which quickly solidifies on another type of substrate material to create the bi-metal structure. On the other hand, solid-state AM joins dissimilar metals at a relatively low temperature. For example, ultrasonic additive manufacturing (UAM) can consolidate thin metal sheets using the principle of solid-state ultrasonic metal welding [6]. Material extrusion (ME) or fused filament fabrication (FFF) is another type of AM method that enables the creation of bi-metal structures. Specifically, filaments comprising of metallic powders and polymer binders are printed using the ME technology, followed by solvent debinding, thermal debinding, and sintering process to achieve the dense, polymer-free parts [7]. The bi-metal structure in a green state is achieved during the printing step by alternating the filament loaded with different types of metal powders, and a co-sintering process is applied on the debound part to form the

* Corresponding author.
E-mail address: fning@binghamton.edu (F. Ning).

https://doi.org/10.1016/j.jmapro.2023.05.025
Received 17 April 2023; Accepted 2 May 2023
Available online 12 May 2023

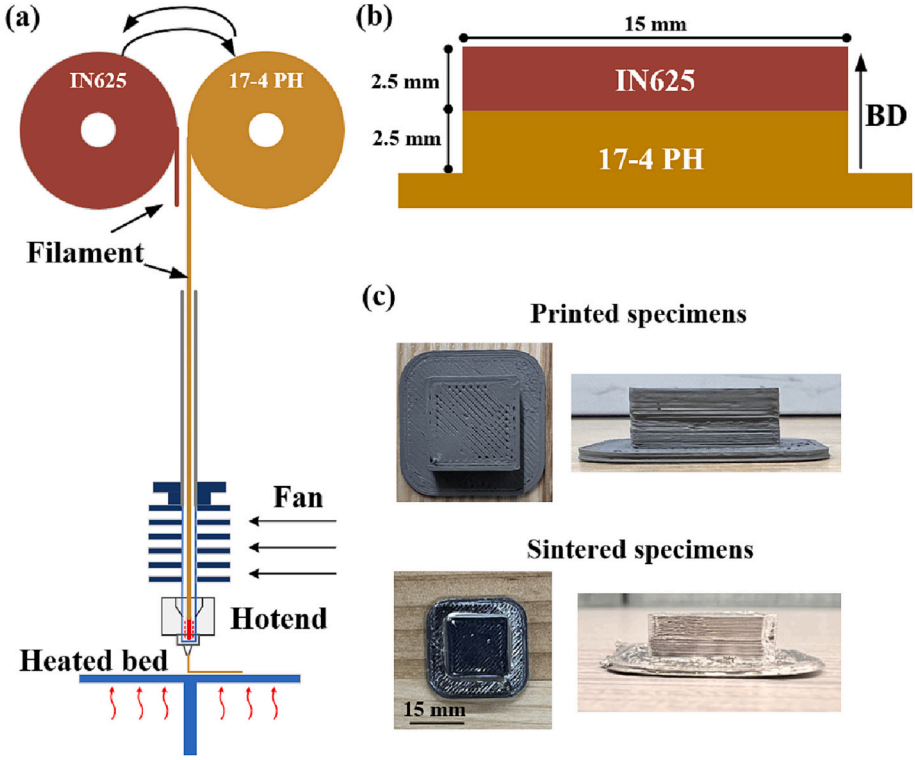

Fig. 1. (a) Illustration of fused filament fabrication of bi-metal material; (b) specimen geometry design for microstructure observation; (c) actual sample photos including the printed green part and final sintered part. (For interpretation of the references to color in this figure legend, the reader is referred to the web version of this article.)

final sintered bi-metal component.

One of the critical issues when building a bi-metal structure is the poor bonding at the interface. As dissimilar materials are joined together, their crystal structure, thermal expansion coefficients, and phase formation behaviors are usually distinct, causing severe cracking or delamination during the building process [1]. The aforementioned two AM approaches have their advantages and drawbacks when addressing this issue. During fusion-based AM, rapid melting and solidification are induced at the interface for both materials, resulting in highly densified interface but manifesting the effects of CTE mismatch that causes the build failure. In the particular DED process, the thermal stress of a Ti-6Al-4 V component deposited on the 410 SS substrate can be four times larger than the single metal alloy, which would lead to brittle failure and cracks [8]. Cracks induced by large thermal gradient at the IN625 – 316L interface have also been reported [3]. An effective strategy could be to introduce another transitional material to reduce thermal stress, thus facilitating the interfacial bonding. For example, Ni—Cr alloys are usually integrated as transition material in the SS and Ti-6Al-4V bi-metal components [8]. In addition, brittle intermetallic phase at the interface could be generated due to the rapid solidification. As reported by Bobbio et al. [9], Fe—Ti and Ni—Ti based intermetallic phases formed at the interface of Invar and Ti-6Al-4V bi-metal components built by DED would cause cracks and build failure. Therefore, ensuring a great solid solution of elements at the interface for single-phase generation is critical to the strong interfacial bonding. Unlike fusion-based AM methods, the solid-state AM processes are operated at a lower processing temperature. As a result, no significant thermal stress or intermetallic phases would be formed during such processes [10]. This allows for a much smoother bi-metal surface free of large thermal cracks and delamination. However, the lack of atomic diffusion because of low temperature induces unsatisfactory bonding as a large number of pores are formed at the interface, causing easy fracture under shear loading along the interface [11]. Post-fabrication heat-treatments including solution treatment and solid-state sintering have been proved to largely enhance the interfacial mechanical strength because they gradually facilitate the interfacial growth due to elongated atomic diffusion [12].

Sintering process is an essential step to build the bi-metal components integrated by the ME process. A long-term holding near melting temperature will be applied to favor the atomic diffusion and densify the metal powders. Theoretically, it has the potential to resolve the interfacial bonding issue encountered by other solid-state AM methodologies, making it a promising approach in building bi-metal components. However, very little study has been conducted on this extrusion-based sintering-assisted category to build bi-metal parts. The only available research was performed by Mousapour et al. [13]. They manufactured low carbon and high carbon steel bi-metal parts via FFF but reached a poor final part quality because the process parameters are not well optimized. Co-sintering process on bi-metal parts built by injection molding or UAM has been reported [4,14], and the interfacial pores can be significantly reduced by adjusting the sintering temperature profile [14]. Therefore, this work aims to provide one of the pioneering investigations to build bi-metal structure following the material extrusion – debinding – sintering path with highly optimized sintering profile. The microstructure and mechanical performance of the 17–4 PH IN625 bi-metal parts will be characterized. The completion of this study envisions the future potential of material extrusion process in building high-quality bi-metal components with high mechanical performance.

2. Experimental setup

2.1. Material fabrication

The 17–4 PH SS and IN625 nickel alloy are both commercially available filaments manufactured by Markforged Corporation. Inside both filaments, metallic powders are mixed with the same binder system including wax and polyethylene. The multi-material green parts were printed using a desktop high temperature FFF printer (Funmat HT

Table 1
Printing parameters for bi-metal green part build up.

Printing parameters	17–4 PH SS	IN625
Nozzle temperature	290 °C	260 °C
Nozzle size	0.4 mm	0.4 mm
Printing speed	30 mm/s	30 mm/s
Layer height	0.1 mm	0.1 mm
Bed temperature	90 °C	90 °C
Chamber temperature	70 °C	70 °C

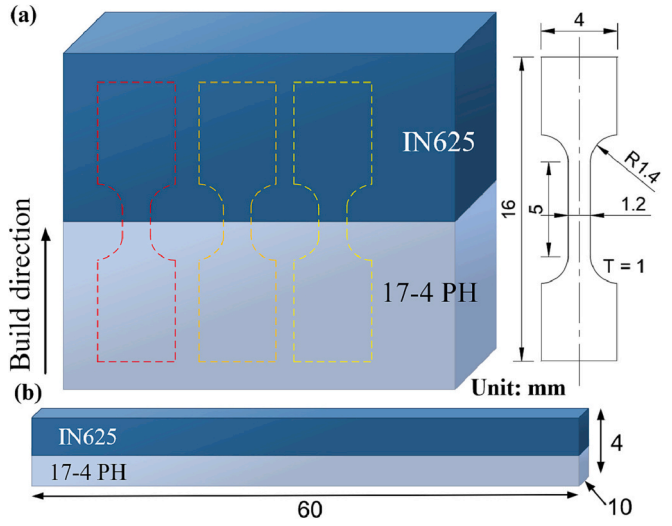

Fig. 2. Illustration of specimen design for (a) tensile and (b) bending tests.

Enhanced, INTAMSYS, China). A graphical illustration of the bi-metal manufacturing process is provided in Fig. 1. A single-nozzle printing scheme with interchangeable filaments was adopted to print the bi-metal "green" part. Single cuboid geometry was printed in 15 × 15 × 5 mm with the material transition placed at the central interface, as shown in Fig. 1. 17–4 PH SS filament was first printed as the raft and base material with 2.5 mm thickness in a layer height of 0.1 mm, then IN625 filament was deposited onto it for another 2.5 mm thickness. The detailed printing parameters for both materials are listed in Table 1. For optimal printing quality, the printing temperature was set at different levels, as shown in Table 1.

The debinding and sintering processes were conducted in the Markforged manufacturing system. Specifically, the printed green parts were immersed in Opteon SF-79 solvent inside a Wash-1 ventilated chamber (Markforged, USA) to dissolve the wax in the binder system. Then, thermal debinding and sintering processes were conducted inside the Sinter-2 furnace (Markforged, USA) under the protective gas mixture of hydrogen and argon. A specific sintering profile for IN625 was selected in this study to sinter the bi-metal component since the melting point of IN625 is slightly lower than that of 17–4 PH. A complete thermal debinding and sintering procedure sustains a total of 29 h.

2.2. Microstruture characterization

The microstructure of the final bi-metal parts along the building direction was observed by optical microscopy (OM) and scanning electron microscopy (SEM). The distribution of pores and grain morphology were both characterized. Specimens were first cut in the cross-section along the building direction and mounted by epoxy. Following the grinding and polishing processes, the sample surface was finally polished by 0.25 μm alumina suspension. Polished specimens were observed under SEM equipped with energy dispersive spectroscopy (EDS) to identify the elemental distribution around the interface. For

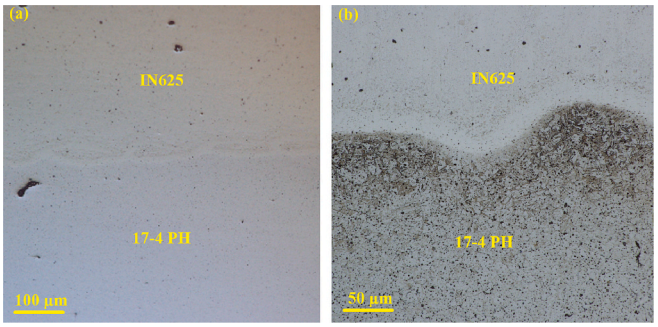

Fig. 3. Microstructure of the 17–4 PH SS and IN625 bi-metal interface showing (a) pore distribution; (b) grain morphology.

OM observation, the sample was further etched by Marble's and Kalling's 2 reagent (ES Laboratory, USA) to reveal the grain morphology. The phase composition of the bi-metal specimen was identified by X-ray diffraction (XRD) method.

2.3. Mechanical testing

Another two types of bi-metal samples were fabricated for testing their mechanical properties. Out-of-plane tensile and bending tests were performed to reveal the interfacial bonding and overall strength of the bi-metal part. The detailed dimensions of the tensile and bending specimens [15] are depicted in Fig. 2. For the tensile test, a universal testing system (ADMET eXpert 4000, USA) was utilized with a loading capacity of 5000 N. The loading speed was set at 1 mm/min according to the ASTM E8 standard [16]. The bending tests were conducted to determine whether delamination would occur during a flexural deformation process [17]. The bi-metal specimen was subjected to a three-point flexural testing using a universal testing equipment (AGS-50kNXD, Shimadzu, Japan) with a loading rate of 1 mm/min following the ASTM E290 standard [18]. A high-speed camera (i-speed 513, iX Cameras, UK) was employed at the front of the bending specimen to record the fracture process at 120 fps. The microhardness of the specimen was tested by a Vickers' hardness tester (LM-310AT, LECO, USA) according to the ASTM E384 standard [19].

3. Results and discussion

3.1. Interfacial microstructure

The metallurgical bonding between the two materials is revealed from the microstructure of the interface, as shown in Fig. 3. Specifically, the polished surface showing the pore distribution is depicted in Fig. 3 (a), where the small pores are distributed uniformly at both the interface and the individual material. Larger dots can be observed near the interface of 17–4 PH portion, which could be due to its relatively low sintering temperature, resulting in insufficient densification. There are no obvious intermetallic phases formed at the interface, aligning well with the results from the literature [20]. The absence of intermetallic phases would contribute to ductile mechanical behavior for the bi-metal part. From Fig. 3(b), we are able to obtain the grain morphology of the 17–4 PH after the surface etching by Marble's and Kalling's reagent. Typical martensitic phases are observed at the interface that results from the precipitation hardening. It is assumed that the phase composition of as-built IN625 is mostly austenitic considering the adoption of appropriate sintering profile [21] but has not been revealed by the chemical etching process. The interfacial band can be observed that shows a lighter color than both materials, indicating that grains are unlikely to form at the interface. The thickness of this band is around 10 μm.

To further understand the element diffusion behavior at the interface during the sintering process, Fig. 4 exhibits the SEM morphology of the

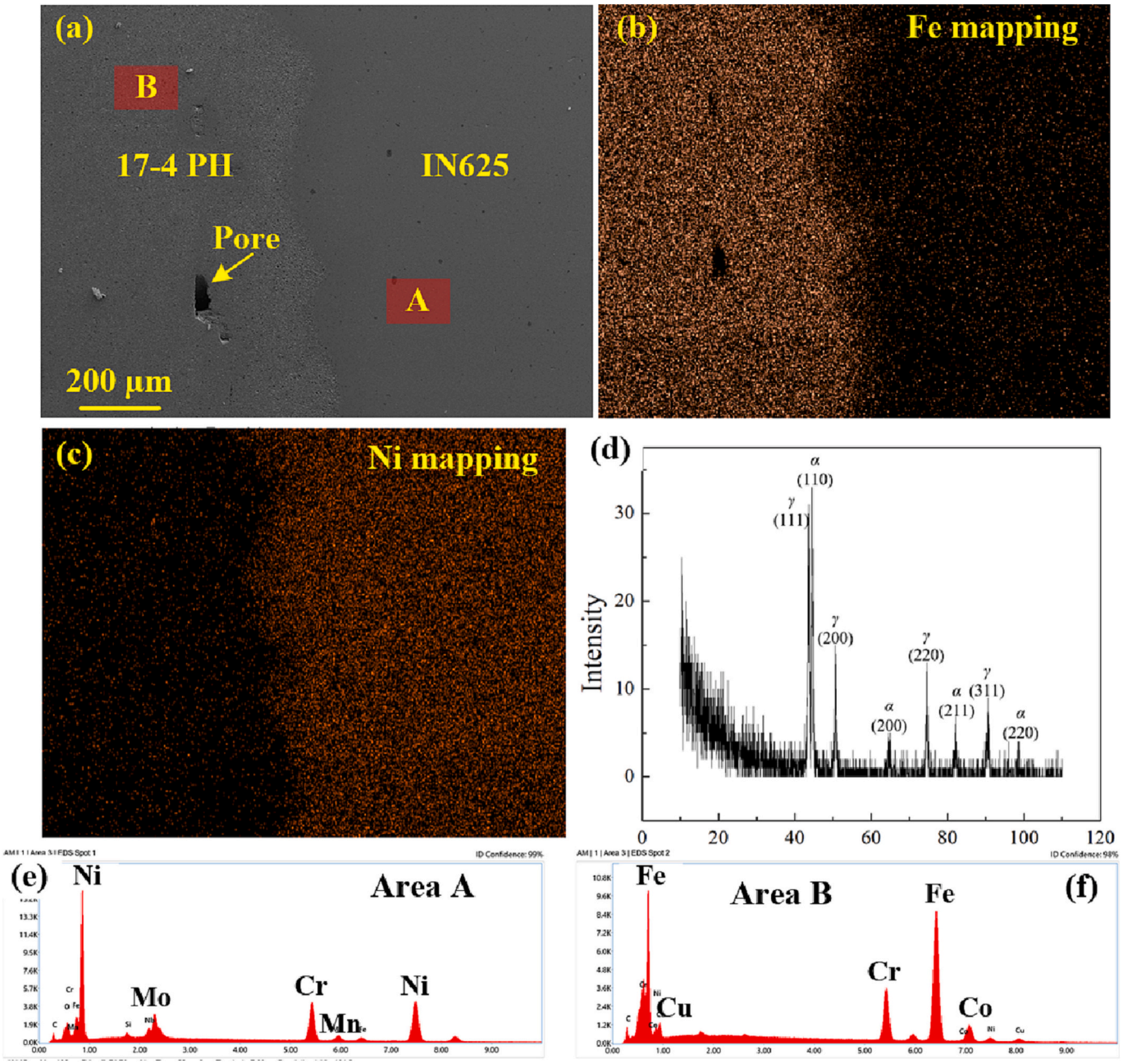

Fig. 4. SEM and XRD results of the 17–4 PH SS and IN625 bi-metal interface. (a) Polished surface showing pores and interface; (b) Fe mapping by EDS; (c) Ni mapping by EDS; (d) XRD pattern; EDS point scanning results of (e) points A and (f) point B in (a).

bi-metal interface and the related EDS element mapping results. In Fig. 4 (a), the winding line of interface is observed with one large pore in the 17–4 PH region. Both materials are determined by measuring the elemental composition of region A and B using EDS. Fig. 4(b) and (c) depicts elemental mapping for the entire surface area for Fe and Ni elements, which are the main elements in the 17–4 PH and IN625, respectively. The XRD spectrum in Fig. 4(d) indicates that no additional phases are generated other than the Ferrite (α phase) from 17–4 PH and the nickel matrix (γ phase) from IN625. Our tests have shown that there is around 3.46 wt% nickel inside the 17–4 PH matrix, whereas around 2.44 wt% iron found inside the IN625 matrix. Nevertheless, it can be seen that the diffusion of Fe element crossing the interface into the IN625 matrix is more remarkable than that of Ni element. An iron composition gradient can be obtained at the interface, spanning around 10 μm thickness, but the nickel element exhibits a much sharper transition at the interface. The reasons for the different diffusion behaviors of elements in the interface might be revealed in a detailed molecular dynamics simulation, which would be beyond the scope of this study. However, the results indicate that the transition zone between sintered 17–4 PH and IN625 bi-metal interface would be mainly comprised of iron and other trace elements.

3.2. *Mechanical properties*

To quantify the interfacial bonding strength and the overall mechanical performance of the bi-metal component, tensile, hardness, and flexural tests were performed. Fig. 5 shows the stress-strain curves of the three bi-metal specimens under tensile tests. They exhibit similar trends of tensile behavior, showing a gradual increase in stress at the beginning, followed by an abrupt fractural failure. The ultimate interfacial

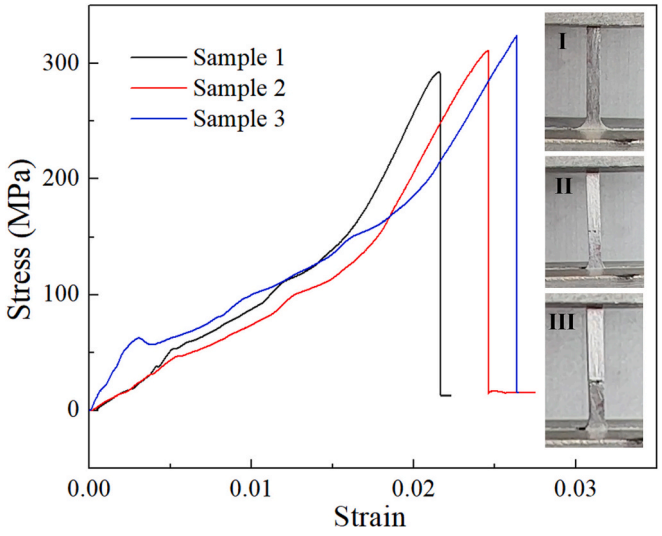

Fig. 5. Stress-strain curves of 17–4 PH and IN625 bi-metal specimens and the macro-scale fracture behavior at three stages.

bonding strength averages around 300 MPa and the elongation is between 2.2 % to 2.6 %. The macro-scale fracture behavior of the tensile specimen is also shown in Fig. 5, including three stages during the tests. At the initial stage (I), the specimen is tightened with the fixture and its surface is ground to improve the surface quality. At the second stage (II) where the specimen is elastically deformed, pores are enlarged, forming a dotting line at the interface that can be identified in the image. The final fracture occurs at the interface after the third stage (III). Brittle failure is indicated as the fracture mostly follows the line of the interface. The tensile test of the bi-metal specimens reveals that the interfacial strength is around 68.6 % of the yield strength of Inconel and stainless steel dissimilar materials manufactured by laser welding, and 62.2 % compared with those built by spark plasma sintering [22,23]. The lower strength could be caused by the large pores existing at the interface as a result of insufficient sintering temperature, especially for the steel portion. Another related reason might be the small transition zone that fails to bond the two alloys strongly. A possible solution is to perform a solid-solution heat treatment to thicken the transition zone and reduce the pore size for creating a stronger interfacial bonding [24].

The results of bending test and failure morphology of the flexural specimen are exhibited in Fig. 6. Fig. 6(a) shows the flexural stress-displacement curves of three specimens. Variations of flexural behavior can be observed from these specimens. Specifically, specimen 1 has the lowest slope of the curve among the three specimens, indicating the smallest modulus, whereas specimen 2 shows the lowest elongation, as the sharp decrease of stress occurs at a displacement near 2.5 mm. The average flexural strengths of the bi-metal structures approach 84.4 % and 82.5 % of the pure 17–4 PH and pure IN625 built by extrusion-based AM, respectively [25,26].

To further evaluate such a difference in the flexural behavior, the macro-scale fractural progress of specimen 2 is studied, as shown in Fig. 6(b) to (d). From a flat multi-material structure, the specimen is gradually bent under the compressive force, and an initial crack has been detected at the bottom surface in Fig. 6(d). This type of crack is usually induced by the tension force at the bottom surface. The crack immediately enlarges and propagates against the loading direction, causing the quick sample failure reflected in the stress-strain curve in Fig. 6(a). Therefore, the quick failure of specimen 2 is due to the crack initiated at the bottom surface of the sample. On the other hand, samples 1 and 2 have more ductile bending behavior, but sample 1 exhibits a significant stress drop before the final failure. This small stress drop

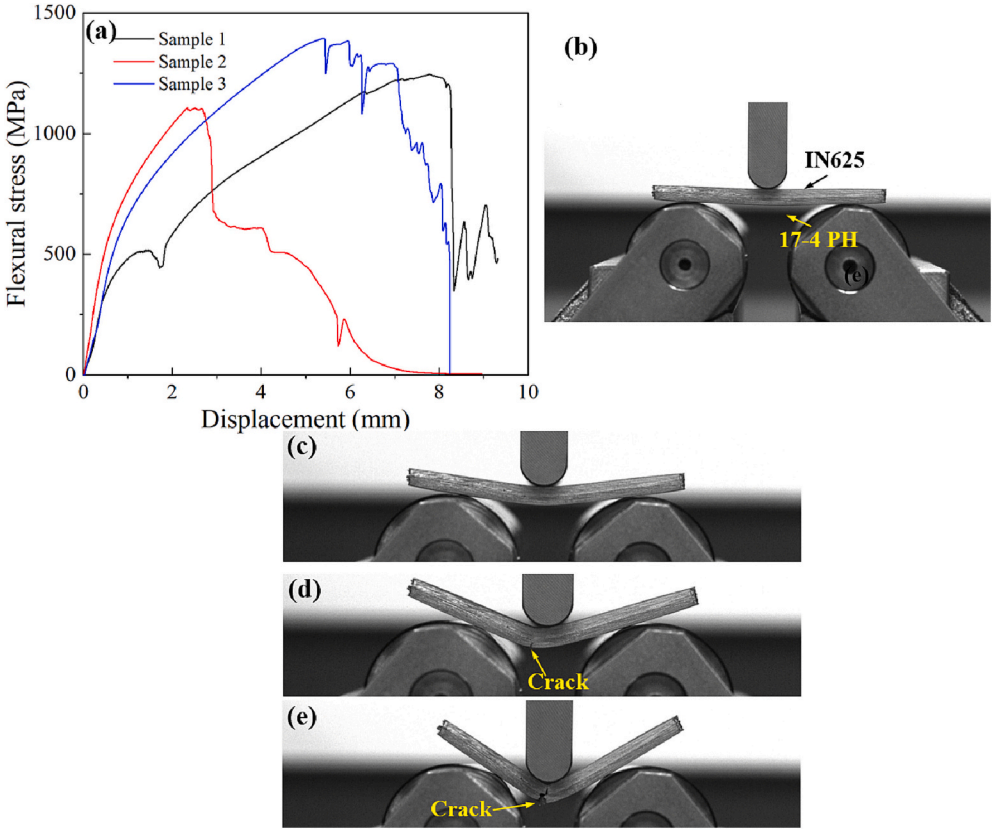

Fig. 6. (a) Stress-displacement curves of three flexural specimens and macroscale fracture morphology for sample 2 at different stages including (b) initial, (c) elastically deformed, (d) large deformation, and (e) final failure.

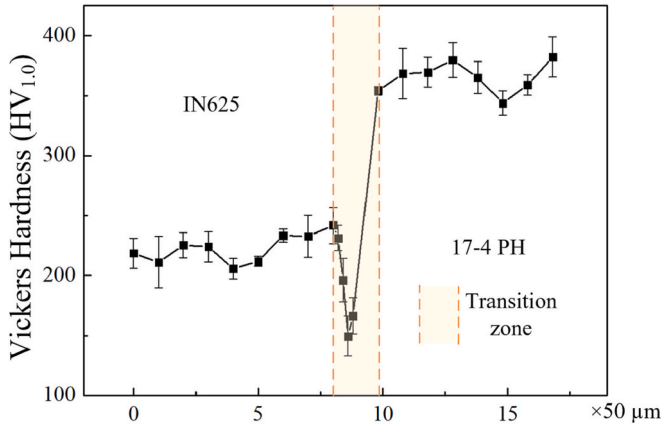

Fig. 7. Vickers hardness of the 17–4 PH and IN625 bi-metal structure.

could be due to the formation of defects (cracks or pores) at microscale, which cannot be observed from macroscopic imaging. This type of failure may lead to a lower modulus of the specimen but would not have a significant impact on its ultimate flexural strength and elongation. In addition, the failure mode for all specimens is matchable with single material as no delamination or interfacial crack is detected. Since no brittle intermetallic phases are formed at the interface, it is indicated that a ductile bond between these two metal materials can be achieved via this manufacturing process.

The mechanical performance of the bi-metal structure is also revealed in microhardness tests. As shown in Fig. 7, the hardness values in IN625 portion, the 17–4 PH portion, and the transition zone were tested with an average step size lower than 10 μm. At the IN625 portion, the hardness value is around 230 HV, whereas the 17–4 PH shows the value above 350 HV. It can be seen that the microhardness for both sintered material is comparable to other reported values [27,28], which suggests that the sintering process is suitable for both individual materials. On the other hand, a transition zone is identified where the hardness value decreases drastically to 150 HV. The thickness of the transition zone determined by the hardness test is about 20 μm. The hardness of the transition zone cannot reach the values of IN625 or 17–4 PH due to the existence of pores and lack of second phases. Therefore, the thin transition zone with low hardness in the 17–4 PH and IN625 bi-metal specimen indicates a weak mechanical strength at the interface, which aligns with the results from the tensile tests.

4. Conclusions

This work provides a pioneering investigation of 17–4 PH SS and IN625 nickel alloy bi-metal fabrication through extrusion-based sintering-assisted additive manufacturing. The microstructure and mechanical properties of the built samples were characterized and tested. The detailed conclusions are listed below:

1. The 17–4 PH and IN625 bi-metal structure was well-bonded after sintering without delamination. Pores were observed at the interface, and the interfacial band thickness was around 10 μm.
2. A composition gradient of iron was measured at the bi-metal interface and the nickel element exhibited a much sharper transition at the interface. The interfacial band would be mainly comprised of iron and other trace elements.
3. The bi-metal interface built by material extrusion AM exhibited a bonding strength below 300 MPa and shows small elongation under the tensile force. However, no delamination is detected for the flexural bi-metal specimen, suggesting a ductile bending behavior.

Future studies can be targeted at deciphering the interfacial bonding mechanism during the printing-debinding-sintering process using the modeling and simulation methodology. Further heat treatments (e.g., solution treatment) can be adopted to reduce the number of pores and enlarge the thickness of the interface, eventually elevating the bonding strength of the bi-metal specimen.

Declaration of competing interest

The authors declare that they have no known competing financial interests or personal relationships that could have appeared to influence the work reported in this paper.

Acknowledgement

This work has been supported by the U.S. National Science Foundation through award CMMI-2224309. The authors also would like to acknowledge the support (Grant # ADLG222) from the Small Scale Systems Integration and Packaging (S3IP) Center of Excellence, funded by New York Empire State Development's Division of Science, Technology and Innovation.

References

[1] Bandyopadhyay A, Heer B. Additive manufacturing of multi-material structures. Mater Sci Eng R Reports 2018;129:1–16.
[2] Li YF, Hong ST, Choi H, Han HN. Solid-state dissimilar joining of stainless steel 316L and inconel 718 alloys by electrically assisted pressure joining. Mater Charact 2019;154:161–8.
[3] Chen N, Khan HA, Wan Z, Lippert J, Sun H, Shang S-L, et al. Microstructural characteristics and crack formation in additively manufactured bimetal material of 316L stainless steel and inconel 625. Addit Manuf 2020;32:101037.
[4] Wolcott PJ, Sridharan N, Babu SS, Miriyev A, Frage N, Dapino MJ. Characterisation of Al–Ti dissimilar material joints fabricated using ultrasonic additive manufacturing. Sci Technol Weld Join 2016;21:114–23.
[5] Heer B, Bandyopadhyay A. Compositionally graded magnetic-nonmagnetic bimetallic structure using laser engineered net shaping. Mater Lett 2018;216:16–9.
[6] Miriyev A, Levy A, Kalabukhov S, Frage N. Interface evolution and shear strength of Al/Ti bi-metals processed by a spark plasma sintering (SPS) apparatus. J Alloys Compd 2016;678:329–36.
[7] Thompson Y, Gonzalez-Gutierrez J, Kukla C, Felfer P. Fused filament fabrication, debinding and sintering as a low cost additive manufacturing method of 316L stainless steel. Addit Manuf 2019;30:100861.
[8] Sahasrabudhe H, Harrison R, Carpenter C, Bandyopadhyay A. Stainless steel to titanium bimetallic structure using LENSTM. Addit Manuf 2015;5:1–8.
[9] Bobbio LD, Otis RA, Borgonia JP, Dillon RP, Shapiro AA, Liu ZK, et al. Additive manufacturing of a functionally graded material from ti-6Al-4V to invar: experimental characterization and thermodynamic calculations. Acta Mater 2017;127:133–42.
[10] Gadakh VS, Badheka VJ, Mulay AS. Solid-state joining of aluminum to titanium: a review. Proc Inst Mech Eng Part L J Mater Des Appl 2021;235:1757–99.
[11] Cepeda-Jiménez CM, Carreño F, Ruano OA, Sarkeeva AA, Kruglov AA, Lutfullin RY. Influence of interfacial defects on the impact toughness of solid state diffusion bonded Ti–6Al–4V alloy based multilayer composites. Mater Sci Eng A 2013;563:28–35.
[12] Baghdadi AH, Rajabi A, Selamat NFM, Sajuri Z, Omar MZ. Effect of post-weld heat treatment on the mechanical behavior and dislocation density of friction stir welded Al6061. Mater Sci Eng A 2019;754:728–34.
[13] Mousapour M, Salmi M, Klemettinen L, Partanen J. Feasibility study of producing multi-metal parts by fused filament fabrication (FFF) technique. J Manuf Process 2021;67:438–46.
[14] Imran M, Deillon L, Sizova I, Neirinck B, Bambach M. Process optimization and study of the co-sintering behaviour of cu-ni multi-material 3D structures fabricated by spark plasma sintering (SPS). Mater Des 2022;223:111210.
[15] Gussev MN, Howard RH, Terrani KA, Field KG. Sub-size tensile specimen design for in-reactor irradiation and post-irradiation testing. Nucl Eng Des 2017;320:298–308.
[16] ASTM E8/E8M-16a. Standard test methods for tension testing of metallic materials. West Conshohocken: ASTM International; 2016.
[17] White SN, Green CC, McMeeking RM. A simple 3-point flexural method for measuring fracture toughness of the dental porcelain to zirconia bond and other brittle bimaterial interfaces. J Prosthodont Res 2020;64:391–6.
[18] ASTM E290-14. Standard test methods for bend testing of material for ductility. West Conshohocken: ASTM International; 2014.
[19] ASTM E384-17. Standard test method for microindentation hardness of materials. West Conshohocken: ASTM International; 2017.
[20] Chen N, Khan HA, Wan Z, Lippert J, Sun H, Shang SL, et al. Microstructural characteristics and crack formation in additively manufactured bimetal material of 316L stainless steel and inconel 625. Addit Manuf 2020;32:101037.

[21] Gonzalez JA, Mireles J, Stafford SW, Perez MA, Terrazas CA, Wicker RB. Characterization of inconel 625 fabricated using powder-bed-based additive manufacturing technologies. J Mater Process Technol 2019;264:200–10.
[22] Dokme F, Kulekci MK, Esme U. Microstructural and mechanical characterization of dissimilar metal welding of Inconel 625 and Aisi 316l. Metals (Basel) 2018:8.
[23] Kumar DP, Kumaran S. Evaluating the microstructural, mechanical, and electrochemical behavior of spark plasma-assisted dissimilar joining of 17-4 PH stainless steel to Inconel 718. J Mater Eng Perform 2022:0–9.
[24] Li Z, Zhao J, Jia F, Liang X, Zhang Q, Yuan X, et al. Interfacial characteristics and mechanical properties of duplex stainless steel bimetal composite by heat treatment. Mater Sci Eng A 2020;787:139513.
[25] Suwanpreecha C, Manonukul A. On the build orientation effect in as-printed and as-sintered bending properties of 17–4PH alloy fabricated by metal fused filament fabrication. Rapid Prototyp J 2022;28:1076–85.
[26] Barwinska I, Kopec M, Łazińska M, Brodecki A, Durejko T, Kowalewski ZL. Suitability of laser engineered net shaping technology for Inconel 625 based parts repair process. Materials (Basel) 2021;14:1–14.
[27] Garcia-Cabezon C, Castro-Sastre MA, Fernandez-Abia AI, Rodriguez-Mendez ML, Martin-Pedrosa F. Microstructure–hardness–corrosion performance of 17–4 precipitation hardening stainless steels processed by selective laser melting in comparison with commercial alloy. Met Mater Int 2022;28:2652–67.
[28] Kotzem D, Beermann L, Awd M, Walther F. Mechanical and microstructural characterization of arc-welded Inconel 625 alloy. Materials (Basel) 2019:12.